NANO LETTERS

Letter

pubs.acs.org/NanoLett

Understanding the Size-Dependent Sodium Storage Properties of $Na_2C_6O_6$-Based Organic Electrodes for Sodium-Ion Batteries

Yaqun Wang,[†,‡] Yu Ding,[†] Lijia Pan,[*,‡] Ye Shi,[†] Zhuanghao Yue,[‡] Yi Shi,[‡] and Guihua Yu[*,†]

[†]Materials Science and Engineering Program and Department of Mechanical Engineering, The University of Texas at Austin, Austin, Texas 78712, United States

[‡]Collaborative Innovation Center of Advanced Microstructures, School of Electronic Science and Engineering, Nanjing University, Nanjing 210093, China

Supporting Information

ABSTRACT: Organic electroactive materials represent a new generation of sustainable energy storage technology due to their unique features including environmental benignity, material sustainability, and highly tailorable properties. Here a carbonyl-based organic salt $Na_2C_6O_6$, sodium rhodizonate (SR) dibasic, is systematically investigated for high-performance sodium-ion batteries. A combination of structural control, electrochemical analysis, and computational simulation show that rational morphological control can lead to significantly improved sodium storage performance. A facile antisolvent method was developed to synthesize microbulk, microrod, and nanorod structured SRs, which exhibit strong size-dependent sodium ion storage properties. The SR nanorod exhibited the best performance to deliver a reversible capacity of ~190 mA h g^{-1} at 0.1 C with over 90% retention after 100 cycles. At a high rate of 10 C, 50% of the capacity can be obtained due to enhanced reaction kinetics, and such high electrochemical activity maintains even at 80 °C. These results demonstrate a generic design route toward high-performance organic-based electrode materials for beyond Li-ion batteries. Using such a biomass-derived organic electrode material enables access to sustainable energy storage devices with low cost, high electrochemical performance and thermal stability.

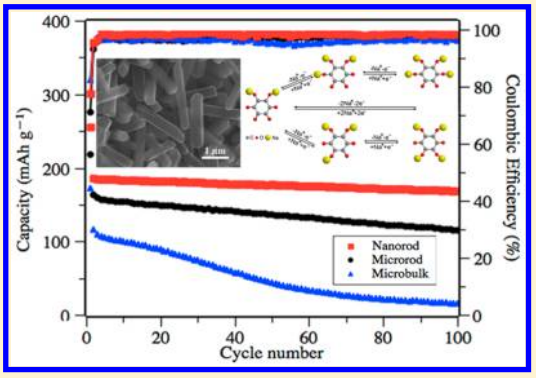

KEYWORDS: *Energy storage, sodium-ion battery, nanostructure, sodium rhodizonate, sustainable materials*

Although lithium-ion battery technology represents a promising energy source for electric vehicles and portable electronics,[1−3] it falls short with regard to price and sustainability criteria because of the high cost and limited availability of lithium sources.[4] Sodium-ion batteries (SIBs) have attracted great attention as an important class of rechargeable batteries because of the large abundance and low cost of Na resources.[5,6] Recently, considerable research efforts have been devoted to developing advanced electrode materials for SIBs.[7] Among them, sulfur,[8,9] selenium,[10,11] O3-type and P2-type sodium metal oxides,[12−14] sodium metal phosphate,[15] and sodium iron sulfate[16] electrodes have demonstrated good electrochemical performance.

Compared to depletable transition-metal inorganic materials that often require energy-intensive processing, biomass-derived organic compounds are promising alternatives as electrode materials for next-generation green energy storage devices.[1−3,17−22] Inspired by the metabolic process resided in organisms depending on redox reactions of biomolecules with specific functional groups such as carboxyl groups and nitroxyl groups, organic materials with different redox centers have been explored to fabricate advanced SIBs.[18−22] Among them, the electroactive carbonyl compounds that mimic the biological electron transfer process of quinone cofactors in nature are considered one of the most intriguing electrode candidates.[23−25] Carbonyl compounds, an important family of cation-insertion electrodes for SIBs, can reversibly insert and release Na ions based on the redox reaction of the carbonyl groups. This type of organic molecules is considered as promising electrode material for SIBs because of their advantageous features including metal-free composition, high reversibility of redox reaction, multielectron reactions, and structural flexibility. Furthermore, they may be obtained from easily accessible natural sources and have highly tailorable properties via molecular design.[26] Recently, various carbonyl compounds have been investigated with regard to their suitability for batteries. For example, Luo et al. used $Na_2C_6O_4$ as an anode that exhibited good capacity stability for 300 cycles.[27] Abouimrane et al. studied carboxylate-based anodes for use in 3.6 V sodium full cells.[28] Okada and Chen et al. used dilithium rhodizonate salt ($Li_2C_6O_6$) for LIBs, which have high potential capacity due to their high-density C═O groups.[18−22] However, their practical capacities and rate performance still

Received: March 4, 2016
Revised: March 31, 2016
Published: April 14, 2016

DOI: 10.1021/acs.nanolett.6b00954
Nano Lett. 2016, 16, 3329−3334

need improving and so do their cycling performances, given the substantial capacity decay upon cycling.[29]

The present study demonstrates the morphological control and size effect of sodium rhodizonate dibasic (SR) when used as a cathode material in rechargeable SIBs. SR nanorod, microrod, and microbulk structured samples were synthesized by a facile antisolvent method and investigated on their size-dependent electrochemical characteristics as SIB electrodes. SR nanorod with uniform diameters of ca. 200 nm, exhibited the best sodium-ion storage property, demonstrating that controlled nanostructuring leads to greatly improved kinetics of electrochemical reactions.[30] The initial discharge capacity of nanorod structured SR can reach ~190 mA h g^{-1} at current density of 0.1 C and retain 90% of its second cycle capacity after 100 cycles. Such SR nanorod can retain over 50% of their capacity at 0.1 C as the current density is increased to 10 C. Furthermore, we investigated the sodiation mechanism of $Na_2C_6O_6$ using cyclic voltammetric analyses, DFT calculations, and ex situ XRD spectra studies. This work constitutes systematic investigation of carbonyl-based organic materials from morphology design, working potential tuning, to computational modeling.

Sodium rhodizonate dibasic features a six-membered ring of carbon atoms with four carbonyl groups and a carbon−carbon double bond (inset of Figure 1a). The four carbonyl groups

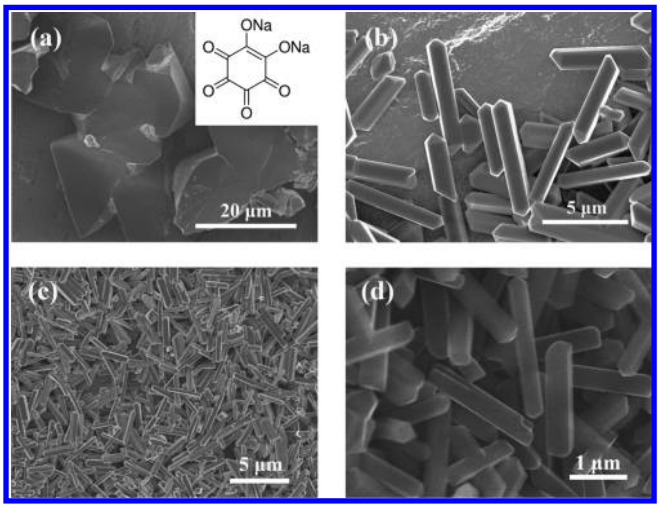

Figure 1. SEM images of SR microbulk (a), microrod (b), and nanorod (c,d) structured samples (inset, molecular structure of the $Na_2C_6O_6$).

provide four actives sites for the redox reactions, while the sodium−oxygen ionic bond can restrain dissolution in carbonate electrolyte owing to high lattice energy in SR salt. Moreover, the dissolution can be further depressed when SR is reduced to highly charged anion-based salt in view of enhanced ionic bond.[20] Thus, the capacity loss due to solubility issue of organic based electrode materials can be mitigated greatly for SR. $Na_2C_6O_6$ has a theoretical capacity of ~250 mA h g^{-1}, corresponding to two carbonyl groups participating in a reversible reaction with sodium ions. Because of the intrinsic insulating properties of $Na_2C_6O_6$, the sample with larger size has a larger transport resistance for Na ions and electrons. Indeed, the large size and small surface areas of $Na_2C_6O_6$ crystal microbulk samples result in poor contacts between SR and conductive carbons, leading to reduced reaction kinetics.

In this study, the microbulk, microrod, and nanorod morphologies of SR were adopted to investigate the size-dependent sodium-ion storage performance and electrochemical sodiation mechanisms. The crystal microbulk structured samples with average 20 μm diameters (Figure 1a) were prepared by recrystallization in water and used as control sample. To improve the sodiation/desodiation kinetics, SR samples with smaller sizes were prepared, such as microrod with an average diameter of ~1.5 μm (Figure 1b) and nanorods with a uniform average diameter of ~200 nm (Figure 1c,d). For the antisolvent crystallization method adopted in our studies, the main driving force for precipitation of crystals is rapid and high supersaturation of SR in ethanol as antisolvent. The controlled growth of nanorod structure is facilitated when ethanol is added into SR aqueous solution. During sonication, the organic salts start to crystallize in a few seconds owing to their poor solubility in the water/ethanol solvent mixture and then self-assemble into nanorods. The diameter of the rods can be controlled by adjusting the concentration of the SR aqueous solution. It has been demonstrated that higher degree of supersaturation usually results in lower Gibbs free energy, which gives rise to faster nucleation rates, and growth of particles take place simultaneously to counteract supersaturation.[31] Accordingly, with higher concentrations the high nucleation rates with relatively slow particle growth would yield precipitation of thinner nanorod.[32] As shown in Figure 1c,d the solution-based as-synthesized nanorod exhibits relatively uniform diameters following sonication.

SR samples of different morphologies were further characterized by X-ray diffraction (XRD). The space group of orthorhombic SR structure is *Fddd* with alternating layers of hexagonal Na cations and rhodizonate anions. In addition to the same crystal structure corroborated by XRD patterns (Supporting Information Figure S1), three SR samples with microbulk, microrod, and nanorod structures also show the same elemental content according to the EDX data (Table S1). The thermal stability of SR samples was also investigated. As shown in TGA curves (Supporting Information Figure S2), SR is thermally stable in air up to 300 °C, which indicates that it could be used as electrode material even at elevated high temperatures.

The electrochemical characteristics of SR samples with different morphologies were compared in the half-cell format with sodium metal as anode. To investigate the redox behavior of SR, cyclic voltammetry (CV) measurements were initially performed in the voltage of 1.6−2.8 V at a scan rate of 0.2 m V/s at ambient temperature (25 °C), as shown in Figure 2. In the first cycle for SR nanorod sample, there is only one peak at 1.80 V during sodiation and two peaks at 1.87 and 2.35 V with two shoulders at 2.11 and 2.63 V during desodiation. However, during the following sodiation/desodiation cycle, the cathodic peak at 1.80 V shifts to a lower voltage of 1.72 V, and three new peaks appear at 2.03, 2.23, and 2.47 V. The anodic peak at 1.87 V also increases slightly to 1.92 V. This result suggests that SR is activated during the first sodiation, which could be observed in many high capacity electrodes with large volume changes, such as croconic acid disodium salt.[33] We also characterized the Na ion diffusion kinetics in light of the difference between two peak potentials in the first cycle. In CV tests, the polarization overpotential refers to the hysteresis in forward and reverse peaks. All these results unveil a size-dependent potential hysteresis in CV scans and the large hysteresis is associated with slow sodiation/desodiation kinetics as the crystal size increases.

DOI: 10.1021/acs.nanolett.6b00954
Nano Lett. 2016, 16, 3329−3334

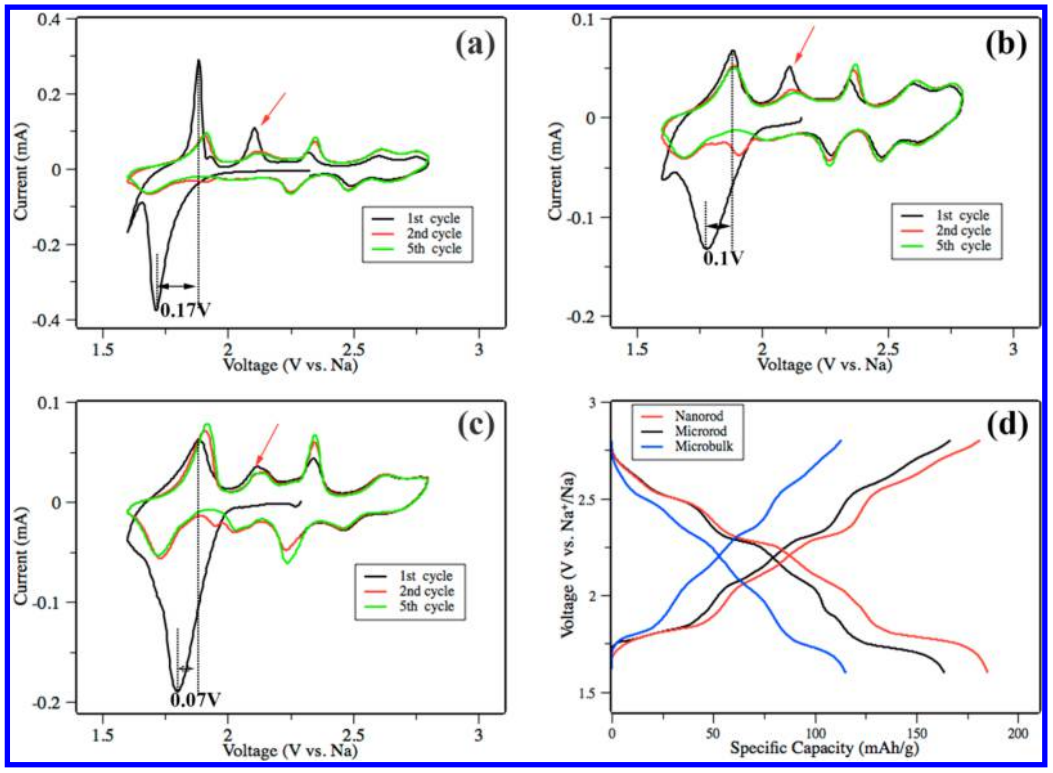

Figure 2. Cyclic voltammograms of SR microbulk (a), microrod (b), and nanorod (c) at 0.2 mV s^{-1} in the potential window from 1.6 to 2.8 V versus Na/Na^+. (d) The second cycle of galvanostatic charge−discharge curves of SR microbulk, microrod, and nanorod samples.

Moreover, the peaks at 2.11 V for SR microbulk and microrod samples decrease during desodiation, while the peak for nanorod is maintained, indicating a reversible reaction.

The charge/discharge profiles for SR microbulk, microrod, and nanorod samples in the second cycle were tested at the rate of 0.1 C (1 C = 250 mA h g^{-1}) and are presented in Figure 2d. The voltage profiles of all three samples exhibit serial voltage plateaus with the first sodiation plateaus being lower than the subsequent sodiation plateaus (Supporting Information Figure S3). These data suggest that all three SR samples experience successive and reversible phase transformations during the first sodiation/desodiation reaction (Supporting Information Figure S4) and stress/strain is introduced in the first sodiation at overpotential due to the large volume expansion. The voltage plateaus and reaction reversibility of SR microbulk, microrod, and nanorod can be clearly observed in CV profiles (Supporting Information Figure S5).

In carbonyl-based electrode materials for SIBs, the redox reaction is associated with insertion/deinsertion of Na ions, and the first-principles density functional theory (DFT) method was employed to unravel the reaction pathways. The calculated total bonding energies in Figure 3 and Table S2 indicate that the four carbonyl groups are favorable redox-active sites for binding of Na ions. The calculated redox potentials are also shown in Table S3. It was found that SR may undergo the sequential one-electron reduction processes at estimated potential of 2.40, 2.13, and 1.96 V or the two-electron process at potential about 2.26 and 2.05 V. The above two results correlate relatively well to the measured potential in Figure 2. The DFT results also explain why more than two redox peaks exist in the two-electron reactions. Because $Na_2C_6O_6$ molecule has four reaction sites, the uptake of sodium ions may take place at different sites, which corresponds to different redox potentials. The calculated potentials in Table S3 also show that

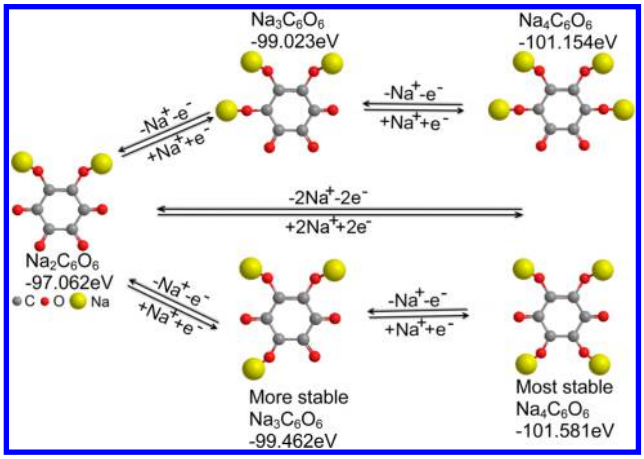

Figure 3. DFT studies of reaction mechanism pathways. Different reaction paths in the sodiation/desodiation of the $Na_2C_6O_6$ electrode were investigated by the DFT calculation.

the one-electron transfer reaction and the two-electron transfer reaction may take place at different redox potentials.

The galvanostatic charge−discharge tests of SR samples were further conducted at a current density of 25 mAh g^{-1} (0.1 C), and the cycling performances of SR electrodes are shown in Figure 4a. The capacity of SR microbulk decreases dramatically, while the microrod SR and nanorod SR show much better cycling stability with nanorod sample yielding the best stability. Because of the intrinsically insulating characteristic of $Na_2C_6O_6$, sodium ions and electrons are not facilely transferred into the internal bulk content. However, the smaller size and larger surface area of the SR nanorod enable sodium ions to be quickly transferred to the inside of $Na_2C_6O_6$. As a result, the

DOI: 10.1021/acs.nanolett.6b00954
Nano Lett. 2016, 16, 3329−3334

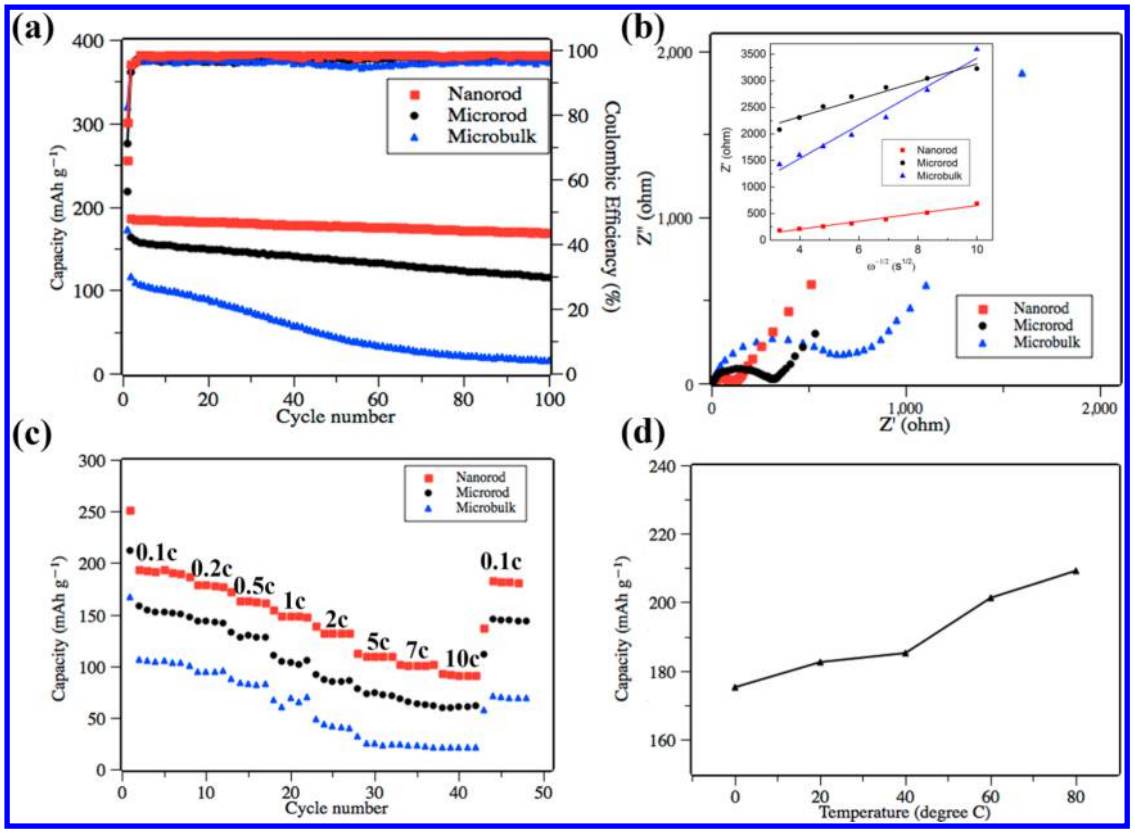

Figure 4. Cycling test (a), EIS spectra with inset figure showing real part of the complex impedance versus $\omega^{-1/2}$ at open circuit potential (b), and rate capability (c) of SR microbulk, microrod, and nanorod samples. (d) Temperature-dependent discharge capacities of the SR nanorod.

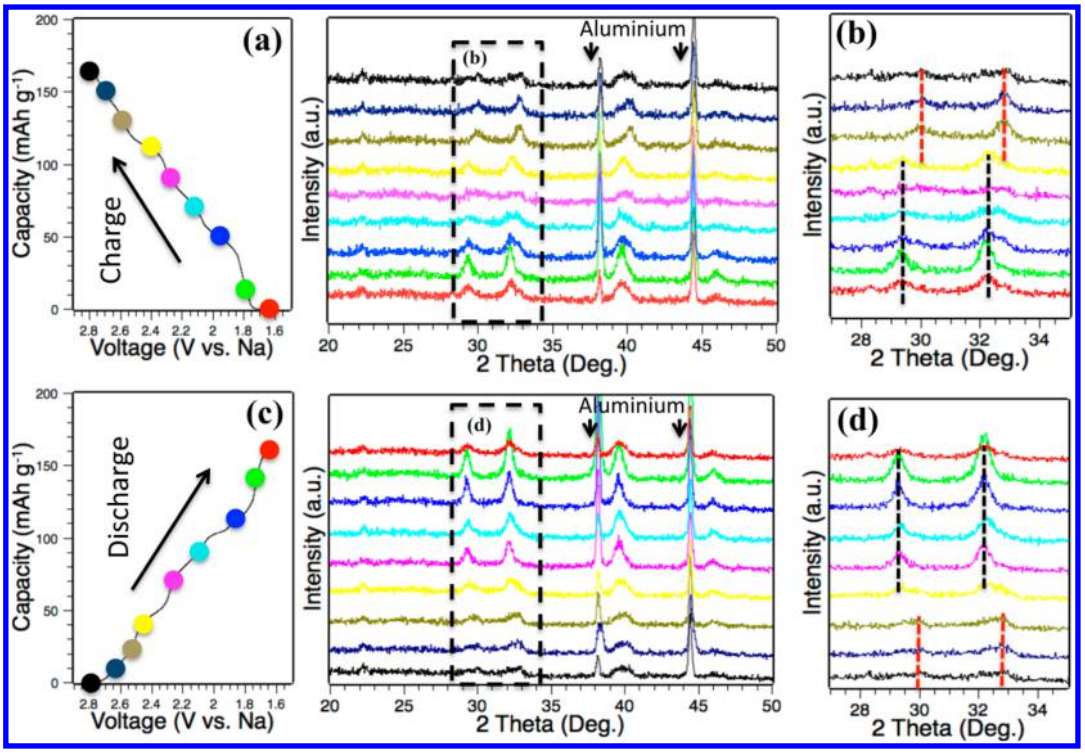

Figure 5. (a) The charge profile of the $Na_2C_6O_6$ electrode is shown in XRD diffractograms obtained during the desodiation process with a magnified region of the XRD diffractograms from 26° to 36° shown in (b). (c) A discharge profile of the $Na_2C_6O_6$ electrode is shown with XRD data obtained during sodiation with a magnified region of the XRD diffractograms from 26° to 36° shown in (d).

capacity and rate performance of SR nanorod are shown to be much higher than those of microbulk and microrod SR.

The reaction kinetics of SR with different sizes were investigated by electrochemical impedance spectroscopy

DOI: 10.1021/acs.nanolett.6b00954
Nano Lett. 2016, 16, 3329−3334

(EIS). The semicircle at high frequency denotes the interface resistance, involving contact and charge transfer resistances, while the low-frequency line represents ion diffusion resistance. As shown in Figure 4b, the interface impedance of SR nanorod is much lower than that of microbulk and microrod SRs, indicating the improved kinetics of nanorod SR. The interface resistance of SR nanorod-based electrodes is ~100 Ω, while the interface resistance for microrod electrode and microbulk SR electrodes have much higher values of 320 and 720 Ω, respectively. The calculated Na ion diffusion coefficient is 7.9×10^{-16} cm^2 s^{-1} at open circuit potential for SR nanorod, compared to 1.96×10^{-16} cm^2 s^{-1} for the microrod SR and 4.36×10^{-17} cm^2 s^{-1} for the microbulk SR based on the slopes of the real part of the impedance versus the square root of frequency (see Methods section for more details in Supporting Information). These results from the EIS test suggest that the enhanced capacity and reaction kinetics of nanorod SR are mainly attributed to the high contact interface area with electrolyte, reduced Na ion transport length and fast Na ion diffusion process.

The rate capability of microbulk, microrod, and nanorod SR samples is compared and shown in Figure 4c. It is noted that SR nanorod exhibits the best rate capability with capacity of 190 mAh g^{-1} at 0.1 C and 95 mAh g^{-1} at 10 C. The high capacity retention is also illustrated in capacity−voltage profiles in Supporting Information Figure S6. When the current density returns to 0.1 C, capacity of SR nanorod comes back to the initial capacity. But for SR microrod and microbulk structures, when increasing the rate from 0.1 to 10 C the capacity decreases from 152 to 60 mAh g^{-1} and from 105 to 42 mAh g^{-1}, respectively. It is clear that the nanorod structure is responsible for high capacity and high power density. Smaller size SR structure could enable larger reaction interphase and faster Na ion diffusion kinetics.

As several key electrochemical characteristics of SIBs such as Na ion diffusion coefficient are temperature dependent, it is also important for electrode materials to have the ability to sustain efficient battery operations over a wide temperature range. Therefore, we evaluated the discharge capacities of our best SR nanorod samples at a current density of 25 mAh g^{-1} at various operating temperatures (Figure 4d). The nanorod SR electrode exhibited a high capacity of ~210 mA h g^{-1} at 80 °C. Notably, a capacity of approximately 175 mA h g^{-1} (~15% decrease in capacity) can be maintained down to temperatures as low as 0 °C.

To further explore the reaction mechanism, the structural changes in the $Na_xC_6O_6$ electrodes during cycling were monitored at various discharged and charged states with XRD spectra, as illustrated in Figure 5. The structure of $Na_2C_6O_6$ is known to belong to the space group *Fddd*.[34] However, the experimental results (Supporting Information Figure S4) illustrate that an irreversible structural phase transition occurs during the first sodiation process. In addition, intercalation reactions in the range of $2.5 < x < 4$ in $Na_xC_6O_6$ are observed. Figure 5a shows that a reversible change of lattice spacing occurs during the second sodiation/desodiation process. In the second full sodiation state, the original peaks of SR at 30.1° and 32.8° shift to 29.4° and 32.2°. The spacing between the layers of atoms increases during sodiation, indicating the insertion of sodium into SR. After desodiation, the XRD peaks of SR shift back to their original positions.

The morphological change of different SR samples was further investigated by SEM imaging before cycling and after 100 cycles. As show in Supporting Information Figure S7, a number of microsized bulk structures were found in the larger-sized SR microbulk, indicating that the volume change during Na-ion insertion/deinsertion would lead to cracking for SR microbulk. A less serious pulverization was observed for SR microrod samples (Figure S7). But for SR nanorods, it is clearly shown that they could accommodate large strain deformation and remain almost intact even after 100 cycles.

In summary, a biomass-derived organic cathode material for rechargeable SIBs based on sodium rhodizonate dibasic with a high density of C═O groups was systematically investigated. SR samples with different sizes were synthesized using the antisolvent method and used as model systems to investigate the size effect on sodium ion storage properties. Excellent cycle performance for SR nanorod electrodes was obtained over the potential range of 1.6−2.8 V, which corresponds to the insertion of less than 2 Na atoms. A stable discharge capacity of the SR nanorod reached ~190 mA h g^{-1} at a current density of 0.1 C and retained over 90% of capacity after 100 charge/discharge cycles. The nanorod structure not only enhances the utilization of active materials but also improves the kinetics of the electrochemical reactions, thus limiting pulverization. This structure enables stable contact between SR and carbon black, which confers the high capacity, high rate capability, and long cycling stability of nanorod-based SIBs. We comprehensively investigated the sodiation mechanism of $Na_2C_6O_6$ using cyclic voltammetry, DFT calculations, and XRD spectra. This combined approach allows for systematic investigation of the carbonyl-based organic SIB cathode materials, including their morphology, working potential, and electrochemical dynamics. With rational structure control, organic nanomaterials based electrodes may lead to the development of environmentally friendly, sustainable, yet high-performance SIBs.

■ ASSOCIATED CONTENT

Supporting Information

The Supporting Information is available free of charge on the ACS Publications website at DOI: 10.1021/acs.nanolett.6b00954.

Detailed experimental procedures and supplementary characterization methods including XRD, SEM, TGA, and DFT calculation of the organic salt. (PDF)

■ AUTHOR INFORMATION

Corresponding Authors

*E-mail: ghyu@austin.utexas.edu.

*E-mail: ljpan@nju.edu.cn.

Author Contributions

Y.W. and Y.D. equally contributed to this work.

Notes

The authors declare no competing financial interest.

■ ACKNOWLEDGMENTS

G.Y. acknowledges the financial support from National Science Foundation (NSF-CMMI-1537894) and 3M Nontenured Faculty Award. L.P. and Y.S. are thankful for financial support from Chinese National Key Fundamental Research Project (2013CB932900), National Natural Science Foundation of China (61229401, 61076017, 60990314), and PAPD program.

■ REFERENCES

(1) Liang, Y.; Tao, Z.; Chen, J. *Adv. Energy Mater.* **2012**, *2*, 742−769.

DOI: 10.1021/acs.nanolett.6b00954
Nano Lett. 2016, 16, 3329−3334

(2) Shi, Y.; Peng, L.; Ding, Y.; Zhao, Y.; Yu, G. *Chem. Soc. Rev.* **2015**, *44*, 6684−6696.
(3) Liu, C.; Li, F.; Ma, L.-P.; Cheng, H.-M. *Adv. Mater.* **2010**, *22*, E28−E62.
(4) Slater, M. D.; Kim, D.; Lee, E.; Johnson, C. S. *Adv. Funct. Mater.* **2013**, *23*, 947−958.
(5) Xiang, X.; Zhang, K.; Chen, J. *Adv. Mater.* **2015**, *27*, 5343−5364.
(6) Yabuuchi, N.; Kubota, K.; Dahbi, M.; Komaba, S. *Chem. Rev.* **2014**, *114*, 11636−11682.
(7) Pan, H.; Hu, Y.-S.; Chen, L. *Energy Environ. Sci.* **2013**, *6*, 2338−2360.
(8) Lu, X.; Kirby, B. W.; Xu, W.; Li, G.; Kim, J. Y.; Lemmon, J. P.; Sprenkle, V. L.; Yang, Z. *Energy Environ. Sci.* **2013**, *6*, 299−306.
(9) Xin, S.; Yin, Y.-X.; Guo, Y.-G.; Wan, L.-J. *Adv. Mater.* **2014**, *26*, 1261−1265.
(10) Abouimrane, A.; Dambournet, D.; Chapman, K. W.; Chupas, P. J.; Weng, W.; Amine, K. *J. Am. Chem. Soc.* **2012**, *134*, 4505−4508.
(11) Luo, C.; Xu, Y.; Zhu, Y.; Liu, Y.; Zheng, S.; Liu, Y.; Langrock, A.; Wang, C. *ACS Nano* **2013**, *7*, 8003−8010.
(12) Billaud, J.; Singh, G.; Armstrong, A. R.; Gonzalo, E.; Roddatis, V.; Armand, M.; Rojo, T.; Bruce, P. G. *Energy Environ. Sci.* **2014**, *7*, 1387−1391.
(13) Guignard, M.; Didier, C.; Darriet, J.; Bordet, P.; Elkaïm, E.; Delmas, C. *Nat. Mater.* **2012**, *12*, 74−80.
(14) Yabuuchi, N.; Kajiyama, M.; Iwatate, J.; Nishikawa, H.; Hitomi, S.; Okuyama, R.; Usui, R.; Yamada, Y.; Komaba, S. *Nat. Mater.* **2012**, *11*, 512−517.
(15) Zhu, Y.; Peng, L.; Chen, D.; Yu, G. *Nano Lett.* **2016**, *16*, 742−747.
(16) Barpanda, P.; Oyama, G.; Nishimura, S.-i.; Chung, S.-C.; Yamada, A. *Nat. Commun.* **2014**, *5*, 4358−4365.
(17) Cheng, F.; Liang, J.; Tao, Z.; Chen, J. *Adv. Mater.* **2011**, *23*, 1695−1715.
(18) Zhao, L.; Zhao, J.; Hu, Y.-S.; Li, H.; Zhou, Z.; Armand, M.; Chen, L. *Adv. Energy Mater.* **2012**, *2*, 962−965.
(19) Wang, S.; Wang, L.; Zhu, Z.; Hu, Z.; Zhao, Q.; Chen, J. *Angew. Chem., Int. Ed.* **2014**, *53*, 5892−5896.
(20) Chen, H.; Armand, M.; Demailly, G.; Dolhem, F.; Poizot, P.; Tarascon, J.-M. *ChemSusChem* **2008**, *1*, 348−355.
(21) Poizot, P.; Dolhem, F. *Energy Environ. Sci.* **2011**, *4*, 2003−2019.
(22) Song, Z.; Zhou, H. *Energy Environ. Sci.* **2013**, *6*, 2280−2301.
(23) Wang, H.; Hu, P.; Yang, J.; Gong, G.; Guo, L.; Chen, X. *Adv. Mater.* **2015**, *27*, 2348−2354.
(24) Wu, X.; Jin, S.; Zhang, Z.; Jiang, L.; Mu, L.; Hu, Y. S.; Li, H.; Chen, X.; Armand, M.; Chen, L. *Sci. Adv.* **2015**, *1*, 1500330.
(25) Ding, Y.; Yu, G. *Angew. Chem., Int. Ed.* **2016**, *55*, 4772−4776.
(26) Seo, D.-H.; Kim, H.; Kim, H.; Goddard, W. A.; Kang, K. *Energy Environ. Sci.* **2011**, *4*, 4938−4941.
(27) Luo, C.; Wang, J.; Fan, X.; Zhu, Y.; Han, F.; Suo, L.; Wang, C. *Nano Energy* **2015**, *13*, 537−545.
(28) Abouimrane, A.; Weng, W.; Eltayeb, H.; Cui, Y.; Niklas, J.; Poluektov, O.; Amine, K. *Energy Environ. Sci.* **2012**, *5*, 9632−9638.
(29) Chihara, K.; Chujo, N.; Kitajou, A.; Okada, S. *Electrochim. Acta* **2013**, *110*, 240−246.
(30) Luo, C.; Huang, R.; Kevorkyants, R.; Pavanello, M.; He, H.; Wang, C. *Nano Lett.* **2014**, *14*, 1596−1602.
(31) Thorat, A. A.; Dalvi, S. V. *Chem. Eng. J.* **2012**, *181−182*, 1−34.
(32) Zhao, Y. S.; Yang, W.; Xiao, D.; Sheng, X.; Yang, X.; Shuai, Z.; Luo, Y.; Yao, J. *Chem. Mater.* **2005**, *17*, 6430−6435.
(33) Luo, C.; Zhu, Y.; Xu, Y.; Liu, Y.; Gao, T.; Wang, J.; Wang, C. *J. Power Sources* **2014**, *250*, 372−378.
(34) Dinnebier, R. E.; Nuss, H.; Jansen, M. *Acta Crystallogr., Sect. E: Struct. Rep. Online* **2005**, *61*, m2148−m2150.

DOI: 10.1021/acs.nanolett.6b00954
Nano Lett. 2016, 16, 3329−3334